

Optimization of Ab-Initio Based Tight-Binding Models

Henrik Dick and Thomas Dahm

Bielefeld University, Physics Department, Postfach 100131, D-33501 Bielefeld, Germany

E-mail: hdick@physik.uni-bielefeld.de

8 August 2025

Abstract.

The electronic structure of solids can routinely be calculated by standard methods like density functional theory. However, in complicated situations like interfaces, grain boundaries or contact geometries one needs to resort to more simplified models of the electronic structure. Tight-binding models are using a reduced set of orbitals and aim to approximate the electronic structure by short range hopping processes. For example, maximally localized Wannier functions are often used for that purpose. However, their accuracy is limited by the need to disentangle the electronic bands. Here, we develop and investigate a different procedure to obtain tight-binding models inspired by machine-learning techniques. The model parameters are optimized in such a way as to reproduce ab-initio band structure data as accurately as possible using an as small as possible number of model parameters. The procedure is shown to result in models with smaller ranges and fewer orbitals than maximally localized Wannier functions but same or even better accuracy. We argue that such a procedure is more useful for automated construction of tight-binding models particularly for large-scale materials calculations.

1. Introduction

A standard method to calculate electronic properties of a crystalline solid is ab-initio band structure calculation based on density functional theory (DFT). In situations, where periodicity is broken, like defects, grain boundaries, interfaces between materials, or complex geometries in electronic devices, ab-initio methods quickly become intractable, however. Ab-initio based tight-binding models have been suggested as a possible simplification that on one hand allows treating much larger and inhomogeneous systems but on the other hand retains the quantum mechanical nature of the bonding in a reduced local real space description.[1, 2, 3] Tight-binding models usually start from a limited set of orbitals at the atomic sites which are used to represent the Hamiltonian of a material in a real space basis.[4] As the matrix elements fall off with distance quickly, tight-binding models are usually restricted in range. The electronic structure can then

be calculated by diagonalization of small matrices representing the Hamiltonian. Tight-binding models for specific materials are not unique as they depend on the chosen real space basis. Different kinds of basis sets can be used, like linear combination of atomic orbitals (LCAO), [4, 5, 6, 7] linear muffin-tin orbitals (LMTO), [8] or Wannier functions, [9, 10, 11] for example. The choice of the basis set influences the range of the tight-binding model that is necessary to accurately represent the electronic structure.

There are two main problems associated with the choice of localized sets of orbitals that have been pointed out in the past: one concerns the automation and the other the accuracy of the models. [12, 13] Before a tight-binding model is constructed from a DFT bandstructure calculation a choice needs to be made, which localized orbitals at which positions are taken. Also, the target bands in the band structure that should be represented by the tight-binding model need to be chosen. These choices usually require human control, which is problematic for automated high-throughput construction of tight-binding models. The other problem is related to the projectability of the bands to the chosen set of localized orbitals. [7] In metallic systems, for example, it is necessary to disentangle the bands before a projection to the localized basis is made, [11, 14] which introduces a systematic error into the tight-binding model and limits its accuracy. This systematic error can be reduced by choosing a larger basis set. However, this requires to repeat the band structure calculation with a larger number of bands and a projection onto a larger set of localized orbitals, which quickly becomes very time-consuming.

A possible way out of these problems has been suggested by Wang et al. [13] The idea is not to specify the atomic orbitals from the beginning but instead let a machine-learning procedure find an optimum number of orbitals. This is achieved with a tight-binding Hamiltonian construction neural network (TBHCNN). The parameters of the network are trained using standard machine learning techniques in such a way as to represent the band structure as accurately as possible with the smallest possible number of parameters. The number of orbitals is gradually increased until a desired accuracy is obtained. On one hand this allows systematic control of accuracy on the other hand such a procedure does not require human control. The feasibility of this procedure was demonstrated for quasi one-dimensional systems (nanoribbons) as well as two-dimensional systems.

In this work we propose a method similar in spirit to the TBHCNN method, however using conjugate gradient optimization of the tight-binding parameters based on first order perturbation theory. While for classical deep neural networks such a method usually does not significantly improve convergence due to the nonlinearities of the network, it turns out that it allows much faster convergence for bandstructures, as it can approach the optimized set of parameters in much larger steps. Also, a preconditioner can be used to further improve convergence.

In section 2 we will briefly introduce tight-binding models along with an analysis of the computational cost needed to diagonalize them. In section 3 we introduce the optimization procedure we propose. As an illustration, in section 4 we apply our procedure to selected three-dimensional materials. Section 5 contains a discussion of the

computation of the corresponding localized orbitals. A comparison with the standard code *wannier90* is made in section 6. As an application of our tight-binding models, the calculation of a Fermi surface is illustrated in section 7. Conclusions are found in section 8.

2. Tight-binding models

In practice the bandstructure of a crystalline solid is described by a countable basis of Bloch-functions. They can be written as superposition of orbitals on a lattice:

$$\Psi_{n,\vec{k}}^\sigma(\vec{r}) = \frac{1}{\sqrt{N}} \sum_{\vec{R}} e^{i\vec{k}\vec{R}} \phi_n^\sigma(\vec{r} - \vec{R}) \quad (1)$$

where ϕ_n^σ represent a set of localized orbitals with spin σ . In the following, the spin will be absorbed into the quantum number n . The Hamiltonian can be represented using this basis [4]

$$\langle \Psi_{n,\vec{k}} | H | \Psi_{m,\vec{k}} \rangle = \sum_{\vec{R}} \exp(i\vec{k}(\vec{R} - \vec{R}')) \int \overline{\phi_n(\vec{r} - \vec{R}')} H \phi_m(\vec{r} - \vec{R}) d^3r$$

Since the sum is taken over the whole lattice, \vec{R}' can be set arbitrarily without changing the result. It is set to zero in the following. In this way the Hamiltonian has been transformed to the tight-binding form where $H_{nm}^{\vec{R}}$ are the tight-binding parameters.

$$\boxed{\langle \Psi_{n,\vec{k}} | H | \Psi_{m,\vec{k}} \rangle = \sum_{\vec{R}} e^{i\vec{k}\vec{R}} H_{nm}^{\vec{R}}} \quad (2)$$

The idea of tight-binding is, that the orbitals are localized and the integrals, which represent $H_{nm}^{\vec{R}}$, are therefore small for large distance $|\vec{R}|$. We consider finite tight-binding models, where the basis has been cut at some point. If the cut bands don't interact with the kept bands, the band energies will be preserved when cutting off the basis. There are different approaches to cutting the basis, depending on whether symmetry should be preserved or not. Slater-Koster tight-binding models [4] use symmetrically complete sets of atomic orbitals and therefore have known transformation properties under rotation and translation of the lattice. Models based on maximally localized Wannier function can have any cut basis and are usually not symmetric. Symmetry adapted maximally localized Wannier functions have been studied in [15].

The bandstructure can be computed by diagonalizing the Hamiltonian. Note that the basis doesn't need to be orthogonal, so a generalized eigenvalue problem has to be solved.

$$H_{nm}(\vec{k}) := \langle \psi_{n,\vec{k}} | H | \psi_{m,\vec{k}} \rangle = \varepsilon_{m,\vec{k}} \langle \psi_{n,\vec{k}} | \psi_{m,\vec{k}} \rangle =: S_{nm}(\vec{k}) \varepsilon_{m,\vec{k}}$$

The matrix of overlaps $S_{nm}(\vec{k})$ [5] can also be represented in tight-binding form and the coefficients will also vanish for large $|\vec{R}|$, because they can be computed using analogous integrals, but without the Hamiltonian. For simplicity, we will assume in the following, that the basis is orthogonal.

2.1. Analytical Properties

The coefficients of the Hamiltonian satisfy $H_{nm}^{\vec{R}} = \overline{H_{mn}^{-\vec{R}}}$, because H is hermitian.

$$\sum_{\vec{R}} e^{i\vec{k}\vec{R}} H_{nm}^{\vec{R}} = \langle \Psi_{n,\vec{k}} | H | \Psi_{m,\vec{k}} \rangle = \overline{\langle \Psi_{m,\vec{k}} | H | \Psi_{n,\vec{k}} \rangle} = \sum_{\vec{R}} e^{-i\vec{k}\vec{R}} \overline{H_{mn}^{\vec{R}}} = \sum_{\vec{R}} e^{i\vec{k}\vec{R}} \overline{H_{mn}^{-\vec{R}}} \quad (3)$$

Tight-binding models are not unique. The view of them is, that they represent the interaction of orbitals, however the orbitals are not fixed. A change of basis with a unitary matrix U_{nm} on the full Hamiltonian yields another tight-binding model with the same bandstructure. In this work we normalize tight-binding models by diagonalizing $H_{nm}(\vec{k} = 0)$, however this is not sufficient to make the model unique. For example with $N \geq 3$ orbitals, tight-binding models exist, which have completely different orbitals, but still the exact same bandstructure:

$$\begin{pmatrix} \cos(k) & 1 & 0 \\ 1 & 1 & 1 \\ 0 & 1 & -\cos(k) \end{pmatrix} \sim \begin{pmatrix} \cos(k) & 1/\sqrt{2} & 1 \\ 1/\sqrt{2} & 1 & 1/\sqrt{2} \\ 1 & 1/\sqrt{2} & -\cos(k) \end{pmatrix}$$

Assuming no neighbor cells \vec{R} are added, these two tight-binding models can not be continuously transformed into one another without changing the bandstructure. In this case there is a discrete set of equivalent models. The optimization algorithm presented below will converge to an arbitrary solution, which makes interpolation between models from different optimization runs impossible even if they possess the same bandstructure, as, like in the example above, there might not be a continuous path from one model to the other without changing the bandstructure.

2.2. Numerical Properties

The tight-binding formalism features $N \times N$ matrices for each \vec{R} , with N being the number of orbitals. In numerical calculations we limit $|\vec{R}|$, such that there is a finite number of these so-called neighbor cells. We only need to store half of them, as the other half is determined by $H_{nm}^{\vec{R}} = \overline{H_{mn}^{-\vec{R}}}$, except for $\vec{R} = 0$. Assuming no more special form and M stored matrices, we can compute the matrix for diagonalization for a single \vec{k} in $(2M+1)N^2 + \mathcal{O}(M)$ floating point operations (FLOPs) for real values, which results in the complexity $\mathcal{O}(MN^2)$. The hermitian matrix diagonalization has the complexity of $\mathcal{O}(N^3) = cN^3$ FLOPs. In total this leads to approximately $(2M+1+cN)N^2 + \mathcal{O}(M)$

FLOPs. To reduce the computational cost of the model, it is therefore essential to use as few orbitals as possible. For the neighbor count, there is more freedom, however note that M grows with the distance $M \sim |\vec{R}|^d$ where the dimension d is usually 3.

If the bandstructure needs to be computed on a full grid of \vec{k} -points with K points, one can use a Fast Fourier-Transform (FFT) to reduce the complexity of computing the $H_{nm}(\vec{k})$ from $\mathcal{O}(KMN^2)$ to $\mathcal{O}(K \ln(K)^d N^2)$, so the diagonalization is again the limiting factor for performance. However, this is not beneficial for the low neighbor counts, which are used in this work.

3. Optimization technique

To find tight-binding models, one has always used fitting procedures of different types. We propose a modified version of the gradient descent algorithm from machine learning. We minimize the weighted loss-function

$$L^2 = \frac{1}{K} \sum_{d,\alpha} w_{d,\alpha} \left| \varepsilon_d(H(\vec{k}_\alpha)) - \varepsilon_d^{\text{ref}}(\vec{k}_\alpha) \right|^2 \quad (4)$$

where $w_{d,\alpha}$ denotes the weights, $\varepsilon_d(H)$ denotes the sorted eigenvalues of the hermitian matrix H and $\varepsilon_d^{\text{ref}}$ denotes the sorted eigenvalues that we are trying to fit. The classical gradient descent algorithm with a learning rate η can be formulated as

$$\begin{aligned} H(\vec{k}_\alpha) &=: U_{id}^\alpha \overline{U_{jd}^\alpha} \varepsilon_d(H(\vec{k}_\alpha)) \\ \varepsilon_d^\alpha &:= \varepsilon_d(H(\vec{k}_\alpha)) \\ H_{nm}'^{\vec{R}} &= H_{nm}^{\vec{R}} - \frac{\eta}{K} U_{md}^\alpha \overline{U_{nd}^\alpha} w_{d,\alpha} \left(\varepsilon_d^\alpha - \varepsilon_d^{\text{ref}}(\vec{k}_\alpha) \right) e^{i\vec{k}_\alpha \vec{R}} \end{aligned} \quad (5)$$

where \vec{k}_α are the \vec{k} -points, at which we are fitting the band structure, U_{nm}^α are the eigenvectors of $H(\vec{k}_\alpha)$ and K is the number of \vec{k} -points. Here $H_{nm}'^{\vec{R}}$ are the updated parameters after a step. This algorithm works in principle, however the choice of η is significant. The usual first acceleration technique is to use a momentum term, which isn't discussed here. The modification of this algorithm in this work is based on the observation, that the change to the bandstructure can be predicted for small steps using first order perturbation theory. In the following $H_{nm}^{\vec{R}_i}$ will be written as H_{nm}^i for better legibility with Einstein sum notation.

$$d\varepsilon_d^\alpha = \overline{U_{nd}^\alpha} U_{md}^\alpha dH_{nm}(\vec{k}_\alpha) = \overline{U_{nd}^\alpha} U_{md}^\alpha e^{i\vec{k}_\alpha \vec{R}_i} dH_{nm}^i \quad (6)$$

It appears, that for bandstructures this prediction also holds for rather large steps. This

would e.g. not be true for the classical deep neural network. Thus, it leads naturally to the idea of finding a least-squares solution to the step dH_{nm}^i given the necessary change $d\varepsilon_d^\alpha = \varepsilon_d^\alpha - \varepsilon_d^{\text{ref}}(\vec{k}_\alpha)$. The least-squares solution can be formulated in the following way:

$$d\varepsilon_d^\alpha = A_{(\alpha d)(inm)} dH_{nm}^i$$

$$A_{(\alpha d)(inm)} := \overline{U_{nd}^\alpha} U_{md}^\alpha e^{i\vec{k}_\alpha \vec{R}_i} \quad (7)$$

$$\tilde{L}^2 = w_{d,\alpha} \left| d\varepsilon_d^\alpha - (\varepsilon_d^{\text{ref}}(\vec{k}_\alpha) - \varepsilon_d^\alpha) \right|^2$$

$$\frac{1}{2} \frac{\partial \tilde{L}^2}{\partial dH_{nm}^i} = w_{d,\alpha} (d\varepsilon_d^\alpha - (\varepsilon_d^{\text{ref}}(\vec{k}_\alpha) - \varepsilon_d^\alpha)) \overline{A}_{(\alpha d)(inm)} \stackrel{!}{=} 0$$

$$\Rightarrow dH_{kl}^j A_{(\alpha d)(jkl)} \overline{A}_{(\alpha d)(inm)} w_{d,\alpha} = w_{d,\alpha} (\varepsilon_d^{\text{ref}}(\vec{k}_\alpha) - \varepsilon_d^\alpha) \overline{A}_{(\alpha d)(inm)} =: v_{inm} \quad (8)$$

$$F_{(jkl)(inm)} := \overline{A}_{(\alpha d)(jkl)} A_{(\alpha d)(inm)} w_{d,\alpha}$$

This is a system of linear equations of the form $F d\vec{H} = \vec{v}$, which needs to be solved to find the step in the coefficients dH_{kl}^i . The matrix F requires $(MN^2)^2$ elements, which is too large to store or invert directly. To simplify this, the action of F can be written as

$$F_{(jkl)(inm)} dH_{nm}^i = \sum_{\alpha} e^{-i\vec{k}_\alpha \vec{R}_j} \sum_d w_{d,\alpha} U_{kd}^\alpha \overline{U_{ld}^\alpha} \sum_{nm} \overline{U_{nd}^\alpha} U_{md}^\alpha \sum_i e^{i\vec{k}_\alpha \vec{R}_i} dH_{nm}^i \quad (9)$$

With this order of summation the action of F can be computed in $K(4MN^2 + 6N^3)$ FLOPs, where K is the number of \vec{k} -points. This is usually the most efficient way to compute the sum. It can easily be parallelized over K . The $\sqrt{w_{d,\alpha}} U_{kd}^\alpha \overline{U_{ld}^\alpha}$ can be precomputed to make it slightly faster within reasonable memory bounds of KN^3 values. For comparison, the diagonalization takes $K(2MN^2 + cN^3)$ FLOPs, where c is a constant depending on the diagonalization procedure. To solve the system of linear equations (9), we use the conjugate gradient (CG) algorithm [16] with a limited number of iteration steps. Due to the step limitation, the CG has the same time scaling as the diagonalization. In practice, we have found that 6 steps of the CG are usually enough to ensure good convergence of the full procedure.

The conjugate gradient method allows the use of a preconditioner L .

$$F\vec{x} = \vec{b} \quad \Leftrightarrow \quad L^\dagger F L \vec{y} = L^\dagger \vec{b}, \quad \vec{x} = L \vec{y}, \quad L \in GL(n, \mathbb{C}) \quad (10)$$

We choose L from the Cholesky decomposition $(e^{i\vec{k}_\alpha(\vec{R}_i - \vec{R}_j)})_{ij}^\dagger = LL^\dagger$. The idea behind this choice is, that in case of $U_{nm}^\alpha = \delta_{nm}$ and in case the above matrix is invertible and not just pseudoinvertible, we get $L^\dagger F L = \mathbb{1}$. This preconditioner is best used, when the \vec{k} -points are not on a regular grid, as it becomes trivial for regular grids.

The numerical implementation of gradient descent, non-preconditioned CG and preconditioned CG are compared in figure 1 for a one dimensional system with two bands and one neighbor term. The reference band values $\varepsilon(k)$ have been sampled from an exact solution in an interval $k \in [-\pi/2, \pi]$ which doesn't cover the full k -space $[-\pi, \pi]$. The reference model is the following model, which has a band crossing:

$$H(k) = \begin{pmatrix} 2\cos(k) & 0 \\ 0 & 1 - 2\cos(k) \end{pmatrix}$$

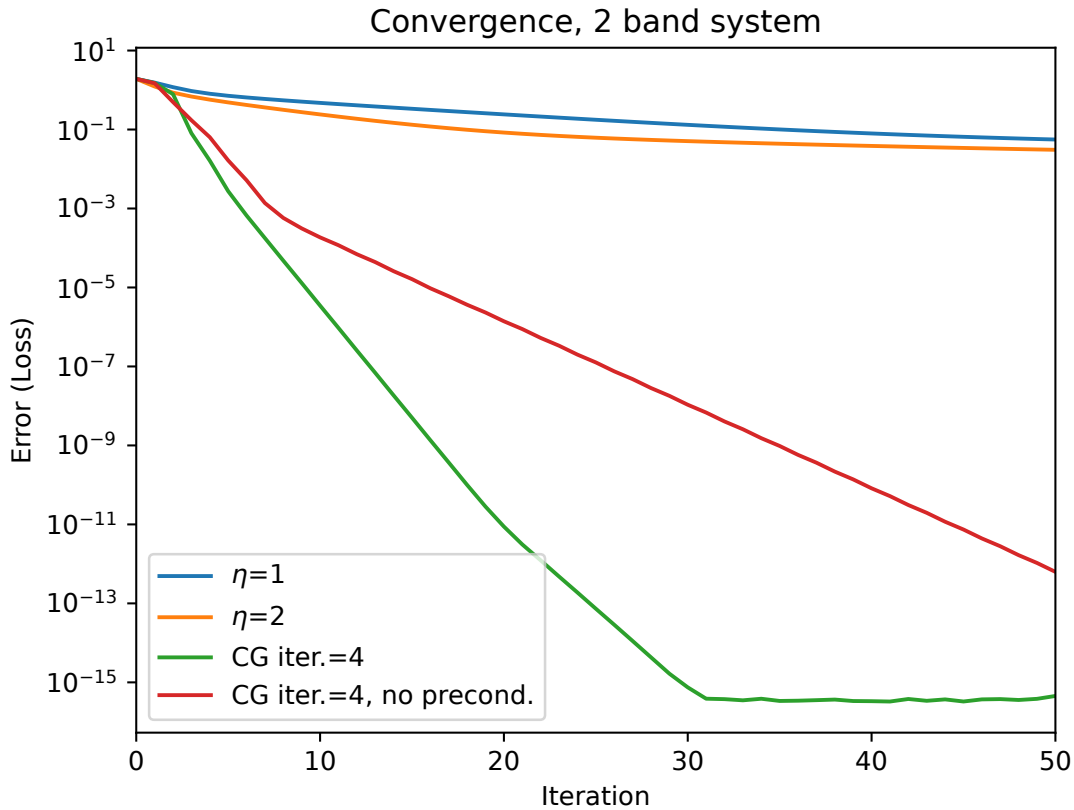


Figure 1. Convergence of Gradient Descent and the improved method based on least squares. The iterations of the x-axis are those of the whole procedure. The CG iterations have been limited to 4.

In the general case the procedure is the following:

1. Start with flat bands with energies matching the reference at the Γ -point. To eliminate starting subspace issues, randomize all parameters by a small amount.
2. Fit the bandstructure with an increasing amount of \vec{k} -points, expanding from the Γ -point. In our fits, the data has been added in 10 equal batches. Each time a new batch is added, one iteration of least-squares fitting is applied.

3. Repeat step 1, 2 several times and use the best fitting model to start the next step. In this work 10 restarts have been used unless explicitly stated otherwise, but in practice 3 would have been sufficient to save some computation time.
4. Fit the model with the least-squares procedure described in this paper. Each time the procedure converges, a small randomization scaled to the current loss is applied, and the fit is continued. We repeated this 10 times. Our convergence criterion was a change of loss smaller than 10^{-3} per iteration. One can get near optimal results (within $\sim 20\%$) much faster by skipping the randomized restarts. It is an open question why they help in the first place.
5. Symmetrically add more neighbors to the model by increasing the maximal radius \vec{R} with \vec{R} in unscaled real space. Then repeat step 4.

We started the procedure with 3 symmetrically equivalent groups of neighbors. For the fitted data we have selected a range of bands and weights by hand, but this could be easily automated by using an energy cutoff. To finalize the fit, one can optionally do one more step using $M = K$ neighbors to eliminate all errors on the reference data. This turns the procedure into an interpolation scheme instead of a fitting scheme.

4. Application to selected materials

We have tested the procedure for various materials with different crystal structures. It has shown to work reliably for all of them to produce good fitting tight-binding models with a low neighbor count. For all the structures we have computed a 24^3 lattice of \vec{k} -points using the DFT package *Quantum Espresso* [17, 18, 19]. Only for TaAs we have enabled spin orbit coupling (SOC). Bismuth would in principle also need SOC for realistic results. We have used KJPAW pseudo-potentials for the PBE GGA-functional from *PSLibrary* [20]. For the self-consistent computation of the electron density, we used a lattice of 10^3 \vec{k} -points. For all fits, we have selected a range of bands by hand and then weighted the top two bands with 0.01 in the loss function. The results are shown in figure 2.

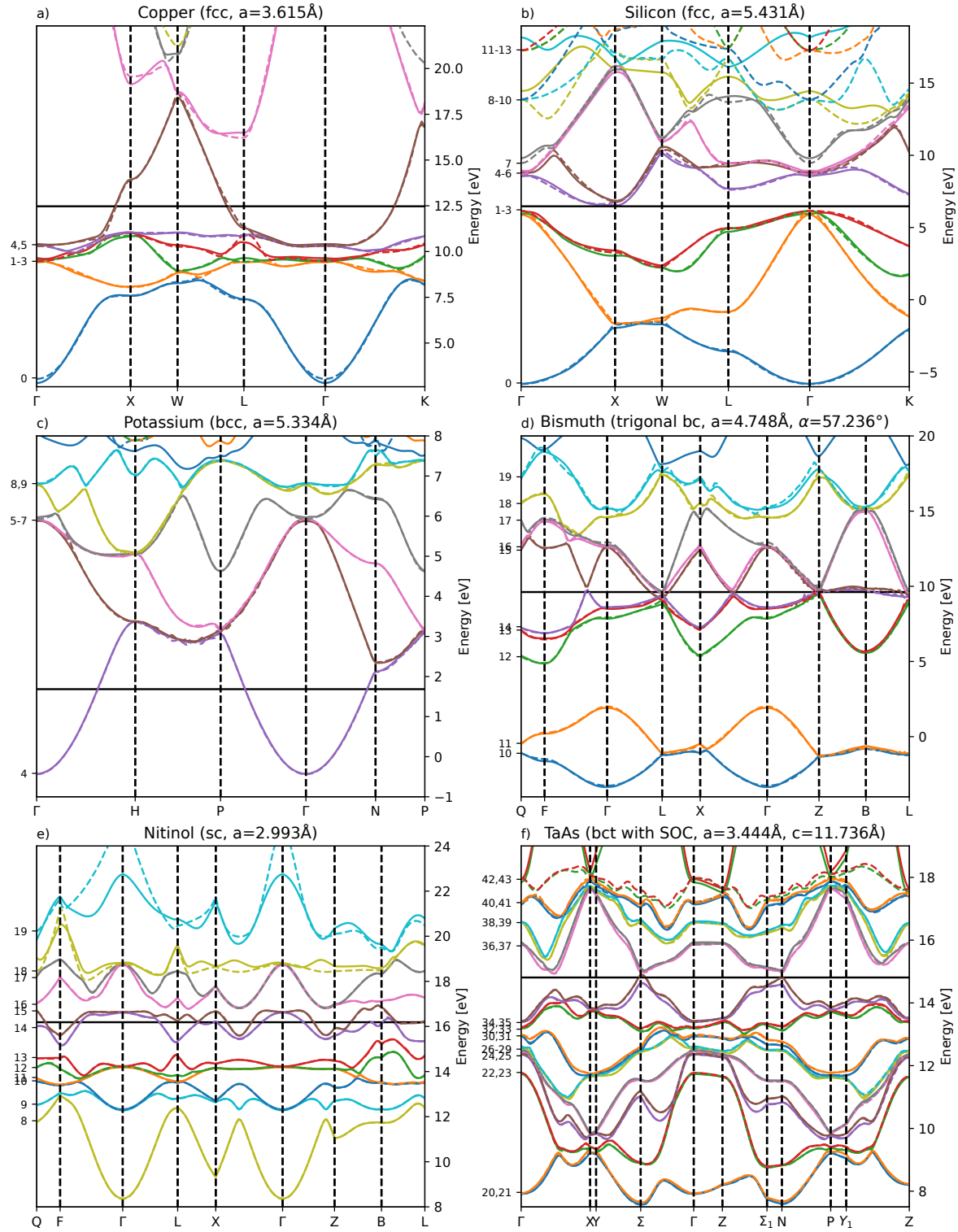


Figure 2. Bandstructures for Cu and Si with neighbors $(0, 1/2, 1/2)$, $(0, 0, 1)$, $(1/2, 1/2, 1)$, K with neighbors $(1/2, 1/2, 1/2)$, $(0, 0, 1)$, $(0, 1, 1)$, Bi with neighbors $(0, 0.958, 0)$, $(0.553, 0, 0.833)$, $(1.106, 0, -0.833)$, NiTi with neighbors $(0, 0, 1)$, $(0, 1, 1)$, $(1, 1, 1)$, $(0, 0, 2)$ and TaAs with cubic symmetrized normalized neighbors $(1/2, 1/2, 1/2)$, $(0, 0, 1)$, $(1/2, 1/2, 3/2)$. The reference DFT data is dashed.

5. Wavefunctions and Orbitals

In other tight-binding procedures, one often gets the orbitals explicitly. [7, 14] The procedure presented here does not provide the orbitals, as the tight-binding model does not contain enough information. There is a relation between the Bloch-eigenfunctions Ψ from DFT and the Orbitals ϕ . The eigenspaces spanned by the tight-binding eigenfunctions and the known eigenfunctions Ψ need to be equal. If the eigenvalues are all unique, the known eigenfunctions equal the tight-binding eigenfunctions up to a phase. They can then be transformed back to the tight-binding basis functions ψ using the unitary matrix $U_{nm}(\vec{k})$, which diagonalizes the tight-binding model. The freedom of choice of Ψ can equivalently be seen as a freedom of choice of $U_{nm}(\vec{k})$.

$$\Psi_{n,\vec{k}}(\vec{r}) = \overline{U_{mn}(\vec{k})} \psi_{m,\vec{k}}(\vec{r})$$

There are two problems with this approach. First, only \vec{k} -points with unique eigenvalues can be used. Second, the phases need to be chosen in a way that minimizes oscillations as discussed in [11] for the application in *Wannier90*. Then one can compute the orbitals from the integral

$$\phi_n(\vec{r}) = \frac{1}{V_{BZ}} \int_{1.BZ} \psi_{n,\vec{k}}(\vec{r}) d\vec{k}$$

Here one needs to use correct integration weights to account for the fact, that highly symmetric \vec{k} -points with non-unique eigenvalues are skipped.

A further procedure similar to *wannier90* [11] is needed to find the best choice of these phases to construct well localized orbitals for given tight-binding models. It has not been implemented in this work.

6. Comparison with Wannier90

We have chosen to compare our method with the established code *wannier90* [14]. Both methods produce asymmetric tight-binding models, however *wannier90* also produces the momentum matrix elements. We have found that due to the disentanglement step in *wannier90* there is a systematic error for metals, which is not present in our method. For comparison, models for the reference materials silicon and copper have been created both using *wannier90* and using our method. The data for these has been computed as in section 4, but with a 8^3 grid for self-consistency and a 16^3 grid without symmetry for the raw data. Both codes don't use any symmetry. The frozen window in *wannier90* has been chosen to cover the bands, which have weight 1 in our fit procedure. Our fits have been computed without the proposed additional randomization step, however some fits with the randomization steps are also included in figure 4 for reference. In *wannier90* it is necessary to choose starting orbitals by hand. For silicon, we used one

s - and 3 p -orbitals each at the two inequivalent atomic positions. For copper, we used 5 d -orbitals at the copper site and two s -orbitals positioned at the copper site and an interatomic site, respectively.

Figure 3 shows the results of *wannier90* and our method for 16 neighbors by plotting the maximal error of the model over the energy range as a kind of histogram. The values are compared using an additional DFT calculation with a 24^3 grid to avoid any overfitting bias. At this neighbor count, the full *wannier90* model has still more precision, however only in some regions and with much more parameters. It also has a high error at 8eV in copper, which is indicative of overfitting. It disappears in the cutoff model, as the cutoff smoothes the function.

To compare our model to *wannier90* it would be unfair to use the loss from (4), as that is what the fit procedure is minimising, while *wannier90* doesn't know about our choice of band weights. Instead, the error metric is chosen to match *wannier90*'s frozen energy window, by only including data points in (4), which are in the frozen window. To make it even more fair to *wannier90*, the bands are not assumed to be sorted and bands can be skipped in some places. This is done by finding the minimal perfect matching of the squared errors. With this definition of the error, figure 4 shows how *wannier90* models compare to our models. The models, which are all fitted on the 16^3 grid, are again evaluated on the 24^3 grid to avoid any overfitting bias. A cutoff has been used on the *wannier90* model, such that terms with $|\vec{R}| > R$ are removed. Our models for different maximal neighbor distances come from saving checkpoints during the fit procedure, where the neighbors are successively added. Note, that the fit procedure will converge against an error of 0 on all bands when given $M \geq K$ neighbors, which turns it into an interpolation method, however on the test dataset with a finer grid it will still have a finite error.

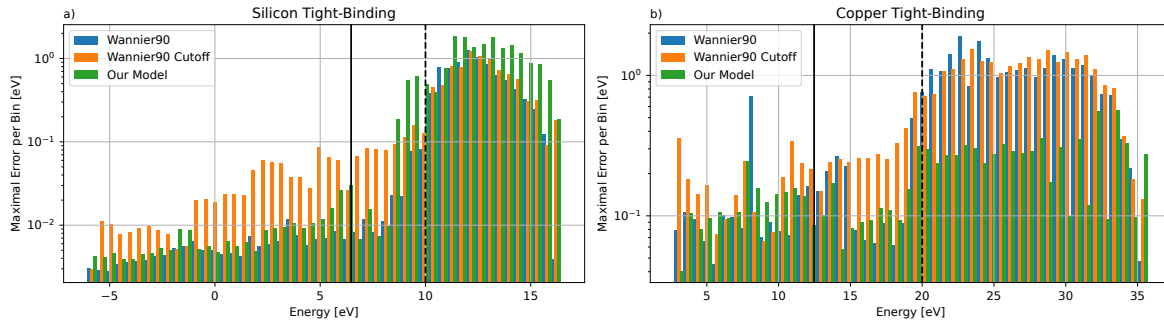


Figure 3. Maximal errors of the tight-binding models for *wannier90* with all neighbors, our model best model with 16 neighbors and cut-off *Wannier90* to match our model in neighbor count. All models are fit on a 16^3 grid, but evaluated on a 24^3 grid. The vertical line is the Fermi energy and the dashed vertical line is the upper edge of the frozen energy window.

The time of all steps has been measured on a PC with an Intel Core i7-8700 (12

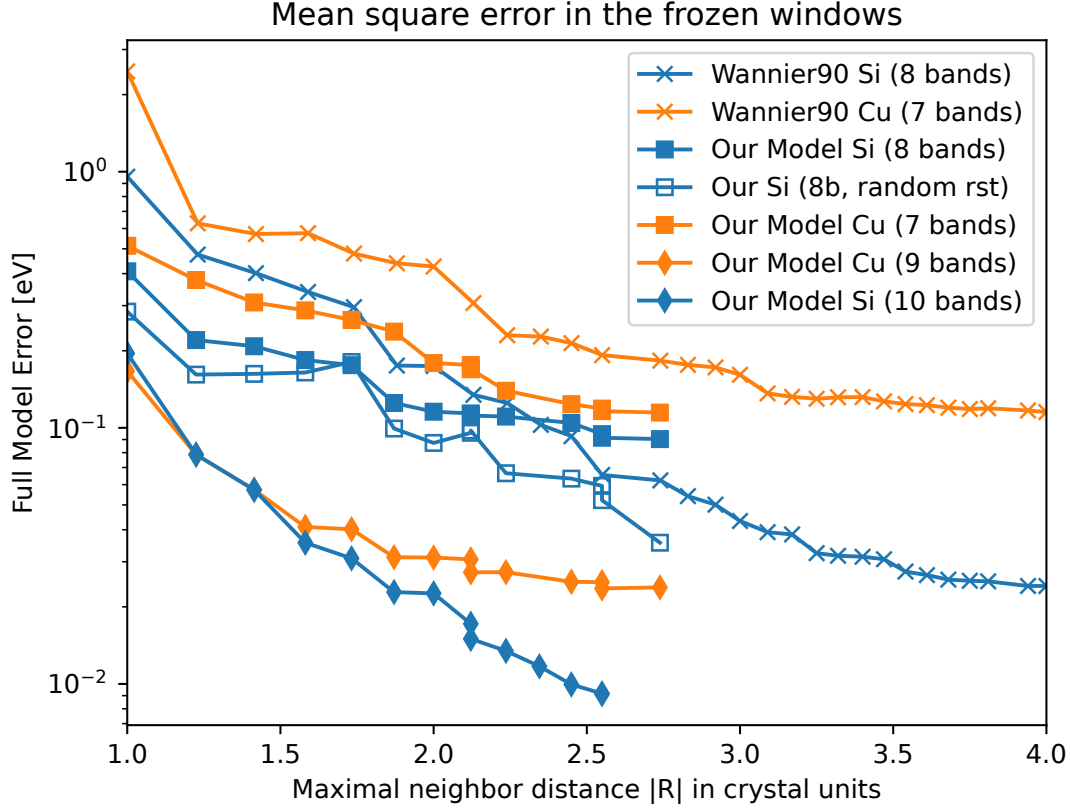


Figure 4. Error of Wannier90 (\times) compared to our method (\square), when used for interpolation with a finite number of neighbors up to some maximal magnitude. The open squares show the result with randomized restarts. The diamonds are results with increased band count.

logical cores, 4.6GHz). The time for the fit of silicon with the described randomized restarts in figure 4 took 38 minutes in total. The time of the fitting procedure scales with $\mathcal{O}(KN^3 + KMN^2)$ where N is the number of orbitals and M is the number of neighbors. For a chosen cutoff R in d dimensions, this results in a scaling of $\mathcal{O}(KN^3 + KN^2R^d)$ per iteration, however the first term usually has the larger constant, as can be seen in figure 5, because the time for each M is roughly equal. The total time scales with $\mathcal{O}(KN^3R^d)$. The space complexity is $\mathcal{O}(MN^2 + KN)$ or $\mathcal{O}(R^dN^2 + KN)$. The wannier90 procedure starts with the program *pw2wannier* to compute the overlap-matrices $A_{nm}^{(k)}$ and $M_{nm}^{(k,b)}$ [10] from the DFT data and then the program *wannier90* to disentangle and compute the maximally localized Wannier-functions. The time complexity for *pw2wannier* is dependent on the energy cutoff, which has been used in the non-self consistent DFT calculation (*nscf*). The energy cutoff determines the cutoff of the plane wave basis. In the following r_G denotes the radius of this cutoff for the plane wave reciprocal lattice vectors \vec{G} . Then we can write the time complexity as $\mathcal{O}(r_G^d KN_r(N + 2dN_r))$ where

K is the number of \vec{k} -points used in the non-symmetric *nscf* calculation, N is the number of Wannier-bands and N_r is the number of non-excluded bands that have been computed in the *nscf* calculation. The space complexity is $\mathcal{O}(KN_r(N + 2dN_r))$. The number of computed bands $N_r \geq N$ is usually chosen to be a few bands more than the used projections and then disentanglement is used. In the test N_r has been chosen as $N_r = N + 2$. Then *wannier90* is run. Without disentanglement, it has the time complexity of $\mathcal{O}(KdN^3)$ for initialization and $\mathcal{O}(KN^3)$ per *wannierization* iteration [9]. The space complexity is $\mathcal{O}(KdN^2)$ due to the need to compute the $M_{nm}^{(k,b)}$ matrix once.

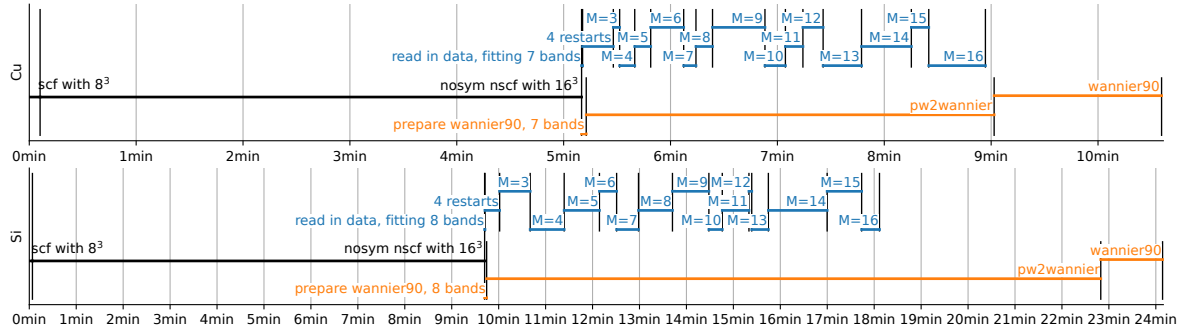


Figure 5. The timing data from the full procedure for *wannier90* and our method (no random restarts) with equal band counts. The non-symmetric DFT calculation *nscf*, which is necessary for *wannier90* and the *pw2wannier90* step, which computes the projections and overlaps for *wannier90*, takes most of the time.

7. Fermi Surface

Since our tight-binding models work with very few neighbors, they produce smooth results for the Fermi-surface. In particular when comparing to roughness minimizing FFT interpolation [21] as implemented in Boltztrap2 [22], our method yields much smoother results, which is ideal for computing group velocities. As seen in figure 6, Boltztrap2 fails to faithfully produce Fermi-surfaces suitable for integration of transport properties depending on derivatives, when there are fine details, as with semimetals. As visible in figure 3b at 8eV, *wannier90* can produce some sharp features as well, which are not contained in the data, because it uses many neighbor terms. However, generally those models behave similar to the models, which are produced in this work, as localized orbitals reduce far neighbor terms, too.

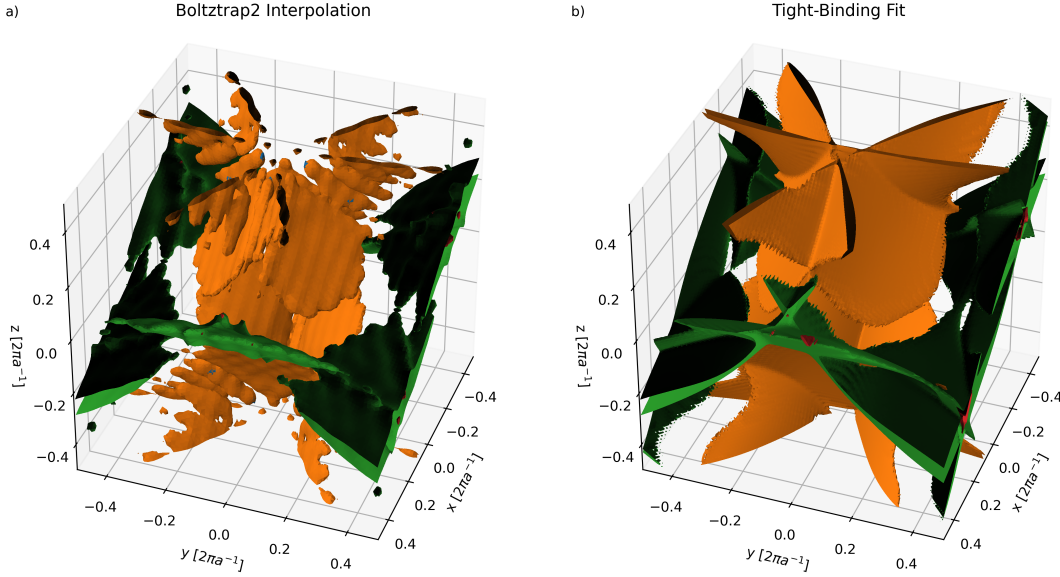


Figure 6. Fermi-surface plots for bismuth using Boltztrap interpolation (left) and a tight-binding fit (right)

8. Conclusion

In this work we devised a procedure to construct tight-binding models for the electronic structure of materials by training on DFT band structures. The method employs least-squares minimization based on first order perturbation theory using conjugate gradients. Special features are a preconditioner, gradual data introduction from the Γ -point, and stochastic refinement by randomized restarts.

In contrast to conventional gradient decent methods, this method features much faster convergence. It also allows systematic control of accuracy, as more neighbors can be added successively until a desired accuracy is reached. We have demonstrated that a high accuracy can be reached already with few neighbors. The resulting tight-binding models possess smooth band structures, which is useful for calculation and interpolation of group velocities and band masses, as well as determination of Fermi surfaces. The models represent the band structure data with a minimum amount of parameters. Orbitals are chosen automatically without the need of human control.

9. Data availability statement

The library code developed and used in this work is available on GitHub at <https://github.com/redweasel/tight-binding/>

10. Acknowledgments

We would like to thank Adrian Braun and Malte Rösner for helpful discussions. We also thank the HPC.NRW Team for their support, as some of the DFT calculations have been done on the Bielefeld GPU Cluster.

References

- [1] Goringe C M, Bowler D R and Hernández E 1997 *Reports on Progress in Physics* **60** 1447 URL <https://dx.doi.org/10.1088/0034-4885/60/12/001>
- [2] Elstner M, Porezag D, Jungnickel G, Elsner J, Haugk M, Frauenheim T, Suhai S and Seifert G 1998 *Phys. Rev. B* **58**(11) 7260–7268 URL <https://doi.org/10.1103/PhysRevB.58.7260>
- [3] Hourahine B, Aradi B, Blum V, Bonafé F, Buccheri A, Camacho C, Cevallos C, Deshayé M Y, Dumitrică T, Dominguez A, Ehlert S, Elstner M, van der Heide T, Hermann J, Irle S, Kranz J J, Köhler C, Kowalczyk T, Kubař T, Lee I S, Lutsker V, Maurer R J, Min S K, Mitchell I, Negre C, Niehaus T A, Niklasson A M N, Page A J, Pecchia A, Penazzi G, Persson M P, Řezáč J, Sánchez C G, Sternberg M, Stöhr M, Stuckenberg F, Tkatchenko A, Yu V W z and Frauenheim T 2020 *The Journal of Chemical Physics* **152** 124101 URL <https://doi.org/10.1063/1.5143190>
- [4] Slater J C and Koster G F 1954 *Phys. Rev.* **94**(6) 1498–1524 URL <https://doi.org/10.1103/PhysRev.94.1498>
- [5] Papaconstantopoulos D A and Mehl M J 2003 *Journal of Physics: Condensed Matter* **15** R413 URL <https://dx.doi.org/10.1088/0953-8984/15/10/201>
- [6] Papaconstantopoulos D A 2015 *Handbook of the Band Structure of Elemental Solids* (New York, NY: Springer) URL <https://doi.org/10.1007/978-1-4419-8264-3>
- [7] Agapito L A, Ismail-Beigi S, Curtarolo S, Fornari M and Nardelli M B 2016 *Phys. Rev. B* **93**(3) 035104 URL <https://doi.org/10.1103/PhysRevB.93.035104>
- [8] Andersen O K and Saha-Dasgupta T 2000 *Phys. Rev. B* **62**(24) R16219–R16222 URL <https://doi.org/10.1103/PhysRevB.62.R16219>
- [9] Marzari N and Vanderbilt D 1997 *Phys. Rev. B* **56**(20) 12847–12865 URL <https://doi.org/10.1103/PhysRevB.56.12847>
- [10] Souza I, Marzari N and Vanderbilt D 2001 *Phys. Rev. B* **65**(3) 035109 URL <https://doi.org/10.1103/PhysRevB.65.035109>
- [11] Marzari N, Mostofi A A, Yates J R, Souza I and Vanderbilt D 2012 *Rev. Mod. Phys.* **84**(4) 1419–1475 URL <https://doi.org/10.1103/RevModPhys.84.1419>
- [12] Gresch D, Wu Q, Winkler G W, Häuselmann R, Troyer M and Soluyanov A A 2018 *Phys. Rev. Mater.* **2**(10) 103805 URL <https://doi.org/10.1103/PhysRevMaterials.2.103805>
- [13] Wang Z, Ye S, Wang H, He J, Huang Q and Chang S 2021 *npj Computational Materials* **7** 11 URL <https://doi.org/10.1038/s41524-020-00490-5>
- [14] Mostofi A A, Yates J R, Lee Y S, Souza I, Vanderbilt D and Marzari N 2008 *Computer Physics Communications* **178** 685–699 URL <https://doi.org/10.1016/j.cpc.2007.11.016>
- [15] Sakuma R 2013 *Phys. Rev. B* **87**(23) 235109 URL <https://doi.org/10.1103/PhysRevB.87.235109>
- [16] Daniel J W 1967 *Numer. Math.* **10** 125–131 ISSN 0029-599X URL <https://doi.org/10.1007/BF02174144>
- [17] Giannozzi P, Andreussi O, Brumme T, Bunau O, Nardelli M B, Calandra M, Car R, Cavazzoni C, Ceresoli D, Cococcioni M, Colonna N, Carnimeo I, Corso A D, de Gironcoli S, Delugas P, Jr R A D, Ferretti A, Floris A, Fratesi G, Fugallo G, Gebauer R, Gerstmann U, Giustino F, Gorni T, Jia J, Kawamura M, Ko H Y, Kokalj A, Küçükbenli E, Lazzeri M, Marsili M, Marzari N, Mauri F, Nguyen N L, Nguyen H V, de-la Roza A O, Paulatto L, Poncé S, Rocca D, Sabatini R, Santra B, Schlipf M, Seitsonen A P, Smogunov A, Timrov I, Thonhauser T, Umari

- P, Vast N, Wu X and Baroni S 2017 *Journal of Physics: Condensed Matter* **29** 465901 URL <https://doi.org/10.1088/1361-648X/aa8f79>
- [18] Giannozzi P, Baroni S, Bonini N, Calandra M, Car R, Cavazzoni C, Ceresoli D, Chiarotti G L, Cococcioni M, Dabo I, Dal Corso A, de Gironcoli S, Fabris S, Fratesi G, Gebauer R, Gerstmann U, Gougoussis C, Kokalj A, Lazzeri M, Martin-Samos L, Marzari N, Mauri F, Mazzarello R, Paolini S, Pasquarello A, Paulatto L, Sbraccia C, Scandolo S, Sclauzero G, Seitsonen A P, Smogunov A, Umari P and Wentzcovitch R M 2009 *Journal of Physics: Condensed Matter* **21** 395502 URL <https://doi.org/10.1088/0953-8984/21/39/395502>
- [19] Giannozzi P, Basergio O, Bonfà P, Brunato D, Car R, Carnimeo I, Cavazzoni C, de Gironcoli S, Delugas P, Ferrari Ruffino F, Ferretti A, Marzari N, Timrov I, Urru A and Baroni S 2020 *The Journal of Chemical Physics* **152** 154105 URL <https://doi.org/10.1063/5.0005082>
- [20] Dal Corso A 2014 *Computational Materials Science* **95** 337–350 URL <https://doi.org/10.1016/j.commatsci.2014.07.043>
- [21] Pickett W E, Krakauer H and Allen P B 1988 *Phys. Rev. B* **38**(4) 2721–2726 URL <https://doi.org/10.1103/PhysRevB.38.2721>
- [22] Madsen G K, Carrete J and Verstraete M J 2018 *Computer Physics Communications* **231** 140–145 URL <http://dx.doi.org/10.1016/j.cpc.2018.05.010>